JOURNAL OF MATERIALS SCIENCE 30 (1995) 2635–2639

Characteristics of phase constitution in the Fe–Al alloy layer of calorized steel pipe

LI YAJIANG, ZHANG YONGLAN, LIOU YUXIAN
Material Engineering Department, Shandong Polytechnic University, Jinan 250014, Shandong, People's Republic of China

Microhardness, aluminium content and phase constitution characteristics in the Fe–Al alloy layer of calorized steel pipe were investigated by optical microscopy, microhardness measurements, SEM, electron probe microanalysis, TEM and X-ray diffractometry, etc. Experimental results indicate that the Fe–Al alloy layer of calorized steel pipe was mainly composed of FeAl phase (20%–36% Al), Fe_3Al phase (13.9%–20% Al) and α-Fe (Al) solid solution, and the microhardness in the Fe–Al alloy layer was 600–310 HM from the surface layer to the inside. There were no higher aluminium content phases, such as brittle $FeAl_2$, Fe_2Al_5 and $FeAl_3$. The ability to resist deformation and the weldability of the calorized steel pipe were remarkably improved.

1. Introduction

Aluminium-coated steel pipes exhibit excellent resistance to oxidation and corrosion in some media, and may remarkably increase the service life of petrochemical equipment. In recent years, numerous investigators have paid close attention to the aluminium-coated steels [1–3]. But, microhardness, aluminium content and phase constitution in the Fe–Al alloy layer of aluminium-coated steels differ greatly for the different aluminizing processes.

This paper presents a study of the latest types of aluminium-coated steel pipe. It is shown that by control of a series of aluminizing process parameters, the thickness, aluminium content and phase constitution of the Fe–Al alloy layer may be effectively controlled, with the elimination of the brittle $FeAl_2$, Fe_2Al_5 and $FeAl_3$ phases in the Fe–Al alloy layer. As a result, the deformation resistance of the aluminium-coated steel may be greatly enhanced and, especially, the weldability may be remarkably improved.

2. Experimental procedure

Base metals used in the test were low-carbon aluminium-coated steel pipe (114 mm diameter, 6 mm wall thickness) and Cr–Mo aluminium-coated steel pipe (114 mm diameter, 10 mm wall thickness). The aluminizing process involved the successive stages of workpiece surface pretreatment, preparation of the primary aluminizing compound, thermal diffusion treatment (by means of electric-induction heating) and surface cleaning of the workpiece, etc. The calorizing parameter was 1050 °C (heating temperature), 15 min (holding time at temperature) and was slow cooling.

Samples of aluminium-coated steel pipes and the weld-joint zone were cut mechanically. Microstructures, thickness and microhardness of the Fe–Al alloy layer were analysed using optical microscopy and a microsclerometer. Aluminium concentration distribution and phase constitution in the coating were further analysed by SEM, electron probe microanalysis (EPMA), TEM and X-ray diffraction. The mechanical properties of the aluminium-coated steel pipes and the weld joints were also measured by tensile and bend testing.

3. Results and discussion

3.1. Microstructure characteristics

The thickness of the Fe–Al alloy layer on the inside and outside walls of low-carbon aluminium-coated steel pipe was 0.15–0.22 and 0.14–0.20 mm, respectively. The thickness of the Fe–Al alloy layer on the inside and outside walls of Cr–Mo aluminium-coated steel pipe was 0.12–0.16 and 0.10–0.14 mm, respectively. The base metal microstructure of the low-carbon aluminium-coated steel pipe exhibited both ferrite and pearlite, there being no other harmful phase present which could affect weldability. The base metal microstructure of Cr–Mo aluminium-coated steel pipe was seen to have a structure of bainite and martensite after normalizing. Annealing was employed to improve further the weldability of Cr–Mo aluminium-coated steel pipe. After annealing, the basic structure was pearlite. Annealing of Cr–Mo aluminium-coated steel pipe greatly improved both the microstructure and other properties, especially that of weldability, whilst properties of the Fe–Al alloy layer were unchanged.

The microhardness of the Fe–Al alloy layer was measured using a microsclerometer using a 50 g load and a load time of 12 s. The microhardness was reduced gradually from the outer surface layer to the

0022–2461

TABLE I Microhardness in the Fe–Al alloy layer

Measuring spot	Distance from surface layer (μm)	Region	Microhardness (HM)
1	15	Coating, outer edge	600
2	30	Coating, outer edge	490
3	45	Coating	475
4	60	Coating	470
5	70	Coating, middle part	460
6	75	Coating, middle part	415
7	90	Coating, middle part	402
8	110	Coating, middle part	395
9	130	Coating	391
10	150	Coating	355
11	180	Coating, boundary with base	350
12	190	Coating, boundary with base	320

base metal (see Table I). When the depth of the Fe–Al alloy layer was less than 60 μm, the microhardness varied in general between 470 and 600 HM. The microhardness near the coating boundary with the base was 320–350 HM. The base metal microhardness was 140 HM for ferrite and 220 HM for pearlite. As a result of this lower microhardness in the Fe–Al alloy layer, the aluminium-coated steel pipes exhibit a good ability to resist deformation.

The oxidation resistance of the Fe–Al alloy layer is determined by the aluminium content. To form a compact and continuous alumite film, 8%–25% aluminium is required to be present at a temperature in excess of 1000 °C, and 5%–8% aluminium is required at 800 °C [4]. The composition of the Fe–Al alloy layer was analysed from the surface of the coating to the interior at successive depths by means of SEM and EPMA. The distance between each point of measurement was 46 μm. The results are presented in Table II. The aluminium content in the Fe–Al alloy layer reduces with increasing depth from the coating. The aluminium content of the surface layer is about 28%. When the depth from the surface layer has reached no more than 140 μm, the aluminium content is in excess of 8%. The effective thickness of the Fe–Al alloy layer can satisfy the necessary requirements for both heat and corrosion resistance.

By analysing microhardness and aluminium content of the Fe–Al alloy layer at different depths, Fe–Al intermetallic compounds which could exist in the coating may be ascertained. The aluminium content and microhardness of different intermetallic compounds in the Fe–Al system are presented in Table III [5, 6].

TABLE II Al and Fe content in the Fe–Al alloy layer

Measuring spot	Distance from surface layer (μm)	Al (wt%)	Fe (wt%)
0	0	28.00	72.00
1	8	26.55	73.05
2	52	21.62	77.87
3	98	16.76	82.59
4	125	9.85	89.46
5	144	6.81	92.56
6	190	1.30	97.45

TABLE III Aluminium content and microhardness of intermetallic compounds in the Fe–Al system

Phase	Al (wt %)		Microhardness (HM)
	According to phase diagram	Chemical analysis	
Fe_3Al	13.87	14.04	350
FeAl	32.57	33.64	640
$FeAl_2$	49.13	49.32	1030
Fe_2Al_5	54.71	54.92	820
$FeAl_3$	59.18	59.40	990
Fe_2Al_7	62.93	63.32	1080

3.2. Phase constitution in the Fe–Al alloy layer

The Fe–Al alloy layer was further analysed in discreet layers with the aid of an X-ray diffractometer, using a copper target. The working voltage was 40 kV and the working current was 150 mA. The experimental results are presented in Figs 1 and 2. The crystal-face spaces (d values) corresponding to the diffraction peaks in the diagrams have been computed. These computed results have been compared with the crystal-face spaces (d values) of FeAl phase, Fe_3Al phase, α-Fe(Al) solid solution and Al_2O_3 which have been published by the Joint Committee on Powder Diffraction Standards (JCPDS) [7], see Table IV. The experimental results indicate that the measured values are close to the d values published by JCPDS.

FeAl (bcc) phase and Fe_3Al (fcc) phase are predominantly present in the Fe–Al alloy layer of this research, other phases, such as $FeAl_2$, Fe_2Al_5 and $FeAl_3$, are not expected to exist in the alloy layer. Usually the aluminium-rich compounds form at the outer surface and compounds progressively richer in iron should form subsequently [5]. However, in many layers, a mixture of compounds forms, some richer in aluminium and some in iron. Further holding of the aluminized sample at 950 °C for 30 min and water quenching made no significant difference to the phase constitution in the Fe–Al alloy layer.

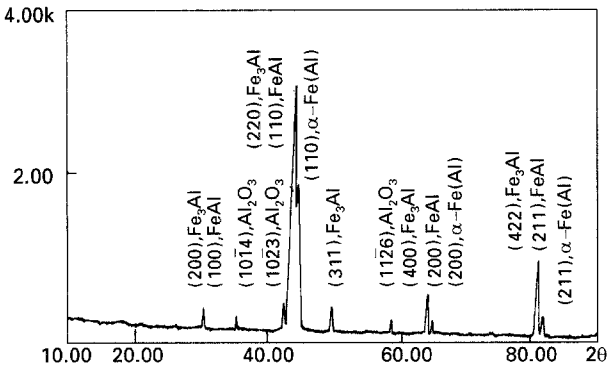

Figure 1 X-ray diffraction diagram of the Fe–Al alloy surface layer (diffraction conditions: copper target, 40 kV, 150 mA).

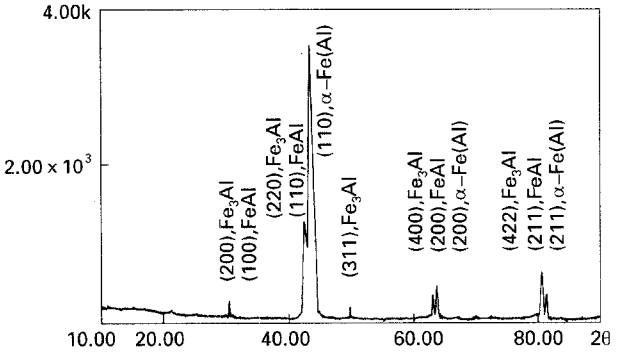

Figure 2 X-ray diffraction diagram from 50 μm below the surface layer (diffraction conditions: copper target, 40 kV, 150 mA).

To clarify further the morphology of the component phases and combined state of the boundary plane in the Fe–Al alloy layer, microstructures of film samples from the Fe–Al alloy layer were analysed by TEM and electron diffraction. TEM morphology, the electron diffraction pattern and schematic index diagrams of the component phases in the Fe–Al alloy layer, taken from the [1 1 1] and [$\bar{1}\,\bar{1}\,\bar{1}$] directions, are shown in Figs 3 and 4, respectively. The black region in the transmission electron micrograph was Fe_3Al and FeAl phases, the white region in the photograph was α-Fe(Al) solid solution which possess b c c structure (the lattice constant is 0.287 nm).

Microstructure morphology of FeAl, Fe_3Al and α-Fe(Al) solid solution near the surface of the Fe–Al alloy layer was analysed by high-resolution multiple SEM and TEM. The results indicate that the component phases were composed of inlaid sub-crystal grains, see Figs 3a and 4a. There was a dislocation twin net at the position of the component phase boundary. No microscopic defects were found, such as pores, cracks and loose, in the FeAl phase, Fe_3Al phase and α-Fe(Al) solid solution. This indicated that the phase constitution of the Fe–Al alloy layer was compact. This is favourable for oxidation resistance and corrosion resistance of the Fe–Al alloy layer of aluminium-coated steel.

Phase construction analysis indicated that the Fe–Al alloy layer of calorized steel pipe was mainly composed of α-Fe(Al) solid solution, Fe_3Al phase, FeAl phase and a small amount of Al_2O_3 (see Table V). Fe_3Al phase and FeAl phase possess characteristics of fine crystal grains, based on features of the polycrystal diffraction pattern.

Further analysis indicated that FeAl phase was not the main component in the Fe–Al coating. Some brittle phases which contained more aluminium, such as $FeAl_2$ (49.13% Al), Fe_2Al_5 (54.71% Al) and $FeAl_3$ (59.18% Al), did not exist in the Fe–Al alloy layer. Weld cracks and deterioration of weld performance formerly caused by these brittle phases in common aluminium-coated steel pipes, were effectively eliminated. As a result, the ability to resist deformation and the weldability of aluminium-coated steel pipes was remarkably improved.

TABLE IV Experimental results of X-ray diffraction for the Fe–Al alloy layer

Measured values	Data from JCPDS											
	FeAl			Fe_3Al			α-Fe(Al)			Al_2O_3		
d (nm)	d (nm)	hkl	I/I_0	d (nm)	hkl	I/I_0	d (nm)	hkl	I/I_0	d (nm)	$hkil$	I/I_0
–	–	–	–	0.334	1 1 1	60	–	–	–	–	–	–
0.291	0.289	1 0 0	12	0.289	2 0 0	50	–	–	–	–	–	–
0.256	–	–	–	–	–	–	–	–	–	0.255	10$\bar{1}$4	90
0.210	–	–	–	–	–	–	–	–	–	0.209	11$\bar{2}$3	100
0.206	0.204	1 1 0	100	0.204	2 2 0	100	–	–	–	–	–	–
0.203	–	–	–	–	–	–	0.203	1 1 0	100	–	–	–
0.180	–	–	–	0.179	3 1 1	20	–	–	–	–	–	–
–	–	–	–	–	–	–	–	–	–	0.174	02$\bar{2}$4	45
–	0.167	1 1 1	4	0.167	2 2 2	10	–	–	–	–	–	–
0.159	–	–	–	–	–	–	–	–	–	0.160	11$\bar{2}$6	80
0.146	0.145	2 0 0	8	0.145	4 0 0	80	–	–	–	–	–	–
0.143	–	–	–	–	–	–	0.143	2 0 0	20	–	–	–
–	–	–	–	–	–	–	–	–	–	0.140	12$\bar{3}$4	30
–	–	–	–	–	–	–	–	–	–	0.137	03$\bar{3}$0	50
0.118	0.118	2 1 1	20	0.118	4 2 2	90	–	–	–	–	–	–
0.116	–	–	–	–	–	–	0.117	2 1 1	30	–	–	–

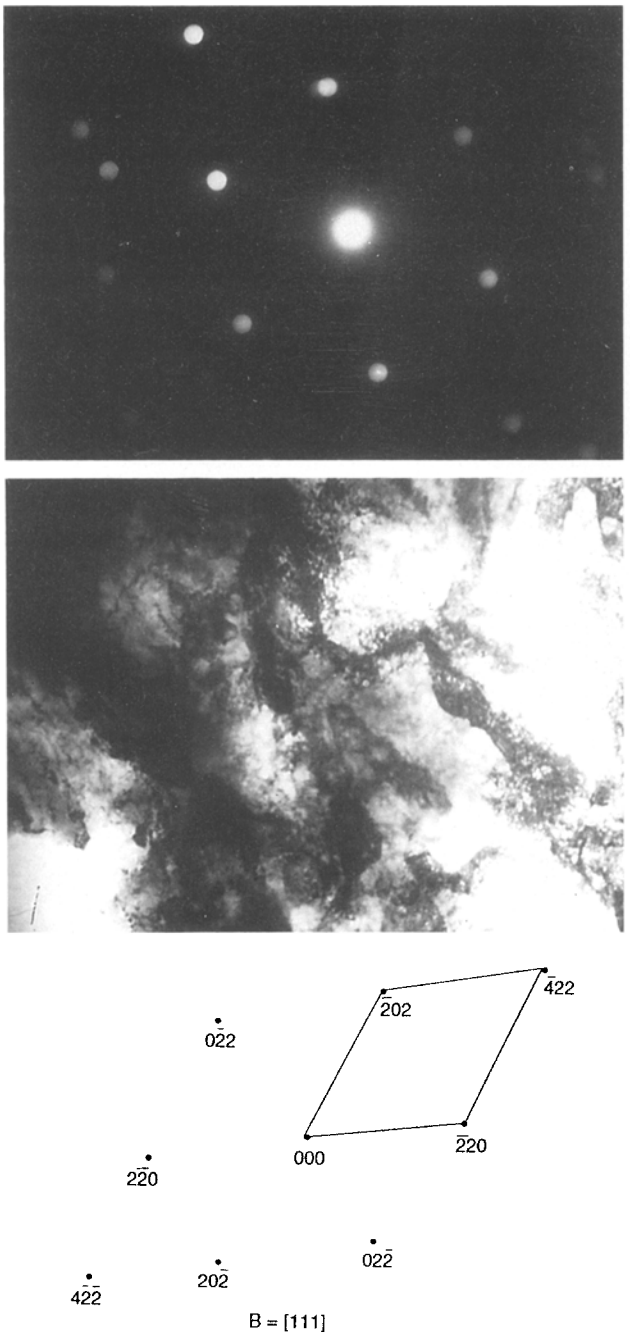

Figure 3 Structure characteristics of Fe_3Al in the Fe Al alloy layer: (a) TEM morphology (× 25 000); (b) electron diffraction pattern; (c) schematic diagram.

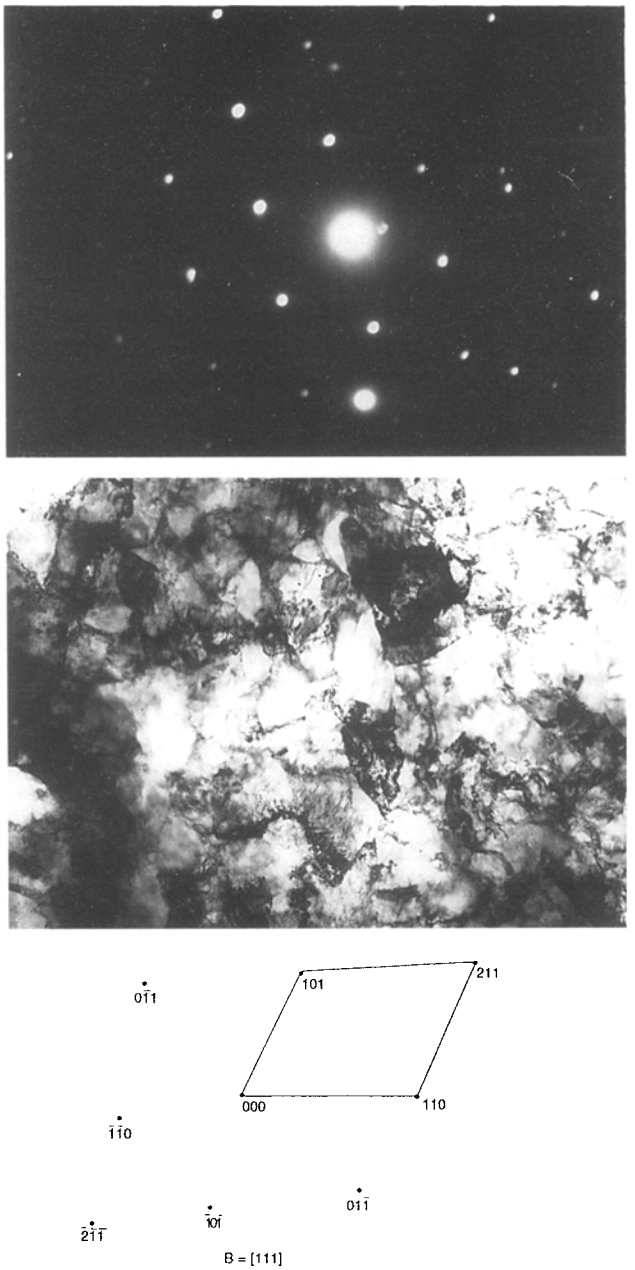

Figure 4 Structure characteristics of FeAl in the alloy layer: (a) TEM morphology (× 20 000); (b) electron diffraction pattern; (c) schematic diagram.

3.3. Deformation resistance ability

Cold-bend tests were made to determine the deformation resistance of the Fe–Al alloy layer on aluminium-coated steel pipe. The original Fe–Al alloy layer on both the inside and outside walls of the calorized steel specimens remained in good condition. Cold-bend angles were 10°–90°, respectively. Specimens after the cold-bend deformation tests were etched in 30% nitric acid–water solution and then examined with a low magnification (× 5–10). Both types of calorized steel pipes may be bent to 30° without any tiny cracks appearing in the Fe–Al alloy layer. The Fe–Al alloy layer of the common aluminium-coated steel pipe produced cracks very easily as a result of the existing brittle phases. The bend specimen of the common aluminium-coated steel pipe may only be bent to about 10°.

TABLE V Phase composition of different diffraction layer faces in the Fe Al alloy layer

Depth from the surface layer (μm)	Phase composition
0	Al_2O_3, FeAl, Fe_3Al and α-Fe(Al) solid solution
50	FeAl, Fe_3Al and α-Fe(Al) solid solution
120	FeAl, Fe_3Al and α-Fe(Al) solid solution

Furthermore, a distorted specimen which had been subjected to an average stress of 500 MPa and an elongation of 8% was cut from the calorized steel pipe. It was subsequently etched in 30% nitric acid–water solution, the Fe–Al alloy layer again being examined with a × 5–10 magnifying glass. No tiny cracks were found.

The results of the cold-bend deformation tests indicated that the Fe–Al alloy layer on the calorized

steel pipes possessed a reasonable degree of deformation resistance and good ductility, both favourable to weldability.

4. Conclusions

1. The average thickness of the Fe–Al alloy layer on the aluminium-coated steel pipes was 0.14–0.22 mm. The aluminium content of the outermost layer was about 28%. The aluminium content in the Fe–Al alloy layer is also reduced with depth. Microhardness in the Fe–Al alloy layer ranged from 600–320 HM taken from the surface to the inner side.

2. X-ray diffraction and TEM results indicated the Fe–Al alloy layer was mainly composed of compact FeAl phase (32.57% Al), Fe_3Al phase (13.87% Al) and α-Fe(Al) solid solution, according to the depth from the surface layer of the coating. There were no brittle $FeAl_2$, Fe_2Al_5 or $FeAl_3$ phases containing more aluminium in the Fe–Al alloy layer. As a result, the adverse influence of these brittle phases on the deformation resistance and the weldability was eliminated.

3. No microscopic defects, such as pores, cracks or loose, were found to exist among FeAl, Fe_3Al and α-Fe(Al) solid solution in the Fe–Al alloy layer. The Fe–Al coating on the calorized steel pipe possessed a reasonable ability to resist deformation. This is favourable to equipment installation and weldability.

References

1. H. OKAMOTO and A. B. PAUL, *Metall. Trans.* **2** (1971) 569.
2. G. E. LINNERT, *Weld. Design Fabric.* **37** (1964) 50.
3. S. C. TJONG, *Werkstoffe Korr.* **37** (1986) 591.
4. F. SAEGUSA and L. LEE, *Corrosion* **22** (1966) 168.
5. ARUNA BAHADUR and O. N. MOHANTY, *Mater. Trans. JIM* **31** (1990) 948.
6. HE KANGSHENG and CAO XIONGFU, "Welding of Dissimilar Metals" (Beijing, 1986).
7. FAN XIONG, "X-ray Metallography" (Tianjing University, 1981)

Received 31 January
and accepted 5 August 1994